




Effect of Co addition on hardness and electrical conductivity of Cu–Si alloys

Chenhui Lei^{1,2}, Huiya Yang^{1,2}, Feng Zhao^{1,2}, Xiaoyang Fang², Youtong Fang², Liang Meng¹, Jiabin Liu^{1,2,*} , and Hongtao Wang^{2,*}

¹School of Materials Science and Engineering, Zhejiang University, Hangzhou 310027, China

²Faculty of Engineering, Center for X-Mechanics, Zhejiang University, Hangzhou 310027, China

Received: 4 April 2021

Accepted: 9 June 2021

Published online:
17 June 2021

© The Author(s), under exclusive licence to Springer Science+Business Media, LLC, part of Springer Nature 2021

ABSTRACT

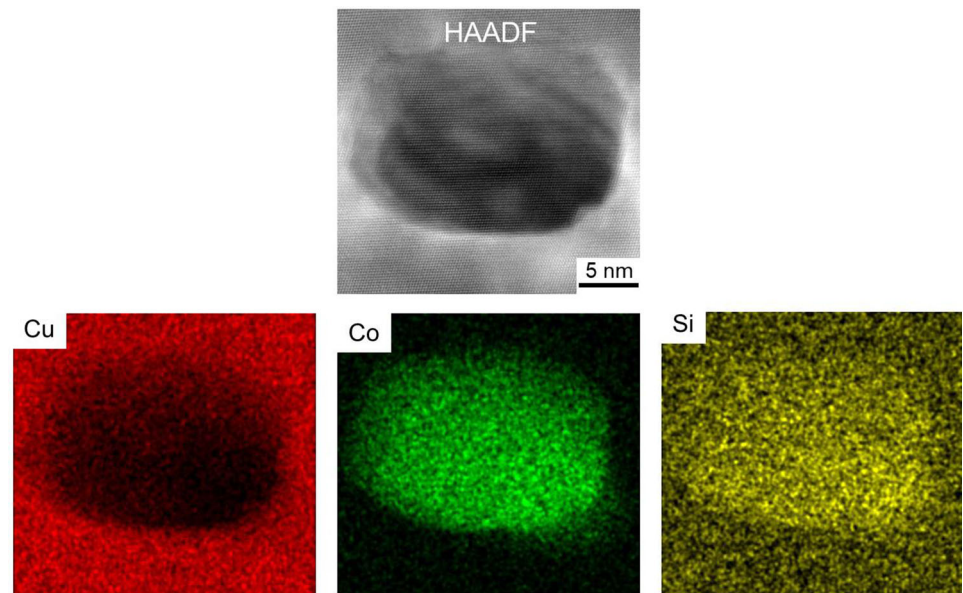
High-strength and high-conductivity Cu alloys are widely required in railway and lead frames. As a conventional element, Si reduces the electrical conductivity of Cu alloys significantly. In this work, Co is introduced into Cu–Si alloys for improving the mechanical and electrical properties. The results show that the Co-containing alloy possesses much higher hardness and conductivity than the Co-free alloys. The added Co reacts with Si to produce high density of CoSi nanoprecipitates that have a semi-coherent interface with the Cu matrix in the aged Cu–Co–Si alloy. The presence of CoSi nanoprecipitates is sufficiently verified by X-ray, energy-dispersive spectrometer and electron diffraction pattern. The formation of CoSi nanoprecipitates can pin dislocation motion, prevent the recrystallization and reduce the Si solute concentration in the Cu matrix. The effects of precipitate hardening and precipitation purification from CoSi phase result in the better performance of the aged Co-containing alloy than the Co-free alloys. The success in Cu–Co–Si alloys opens a door to overcome the disadvantage of Si alloying in Cu-based alloys.

Handling Editor: Catalin Croitoru.

Address correspondence to E-mail: liujiabin@zju.edu.cn; htw@zju.edu.cn

<https://doi.org/10.1007/s10853-021-06251-z>

GRAPHICAL ABSTRACT



Introduction

Cu alloys have excellent electrical and thermal conductivity and are widely used in electrical connectors [1–3] and heat sinks for nuclear fusion [4–6]. Besides the conductivity, mechanical properties are highly required for the Cu alloys used as railway contact wires [7, 8] and lead frames [9–11]. Many Cu alloys containing two and even more alloying elements are developed to achieve high strength and conductivity [12–14].

Si is one of the common alloying element in Cu alloys. There are two advantages of Si alloying. First is that the solute Si in Cu lattice produces a strong solution strengthening effect. The second is that the Si decreases the surface tension and improves the fluidity of Cu melt. However, the electrical conductivity of the Cu matrix is significantly deteriorated by Si addition, which is a serious disadvantage of Si alloying [15]. Since the equilibrium solubility of Si in Cu lattice is as high as 4.6 wt% at an aging temperature of 450 °C [16], the Cu–Si solid solution is difficult to precipitate Si-rich particles by the

conventional aging. It is a challenge to separate the solute Si out of the Cu lattice as complete as possible, which is of supreme importance to achieve high conductivity for Cu alloys. Ni element is concomitantly added with Si to prepare high-strength and moderate-conductivity Cu–Ni–Si alloys because β -Ni₃Si or δ -Ni₂Si compounds can be precipitated [11, 17, 18]. Due to the precipitation, the electrical conductivity of the Cu–Ni–Si alloys is recovered and the solution strengthening effect is compensated by the precipitation hardening effect. Therefore, most of the reported Cu–Ni–Si alloys have high strength and relatively good electrical conductivity [19–21]. However, Ni has limitless solubility in Cu matrix [22]. Both Ni and Si are favorite to remain as dissolved atoms in Cu lattice instead of compounds. It is difficult to ascertain the exact Ni content. The excess Ni dissolved in Cu lattice also deteriorates the electrical conductivity while the skimpy Ni content makes a slight strengthening benefit [23].

Co is able to react with Si to form CoSi and Co₂Si compounds. Besides, the equilibrium solubility of Co in the Cu matrix at 450 °C is close to 0 wt% [24]. Even excess Co is co-added with Si in the Cu matrix, the

residual Co would easily form Co-rich precipitates instead of the solute Co. Several studies adopted this strategy and improved the electrical conductivity of Cu–Si–X alloys. Sun et al. [25] prepared a Cu–Cr alloy with Co and Si additions together and achieved a high hardness (214.6 HV) along with a good electrical conductivity (41.6% IACS). Zhao et al. [26] found that the addition of Co into Cu–Ni–Si alloys resulted in a high hardness of 250 HV and an improved electrical conductivity of 43% IACS. Chen et al. [27] prepared a Cu–2.5 wt% Co–0.5 wt% Si alloy and obtained a peak electrical conductivity of 47.90% IACS along with a hardness of 198.2 HV.

The orthorhombic Co_2Si precipitate was considered as the equilibrium phase during the aging process [28]. Lendvai et al. [29] studied the precipitation process of the Co_2Si in Cu–Co–Si alloys and pointed out that the clustering of Co atoms initiated the precipitation of Si, and so Co_2Si particles were finally formed. Sun et al. [25] studied the precipitation process in the Cu–1 wt% Cr–1 wt% Co–0.6 wt% Si alloy and found that the Co_2Si and Cr precipitates were precipitated from the Cu matrix during aging process.

Compared to the abundant reports on the Co_2Si precipitate, little attention was paid to the CoSi precipitate. The only study of the CoSi precipitates coexisting with the Co_2Si precipitates was reported by Geng et al. [24] in a Cu–1 wt% Co–0.65 wt% Si alloy. However, the formation mechanism of the CoSi phase and the corresponding influence of the CoSi precipitates on the properties of Cu–Co–Si alloys still remain unclear.

In this work, the atomic ratio of Co and Si was controlled to generate CoSi precipitates in the Cu–Co–Si alloy. The influence of CoSi precipitates on the

microstructure, hardness and electrical conductivity of the designed alloy is investigated.

Experimental procedures

When using empirical methods for composition design of the alloy, the complexity in the identification of phases increases with an increase in the number of elements in the system [30]. Here, PANDAT softwareTM, for multicomponent phase diagram calculation from CompuTherm, LLC® was used for the calculation of the phase diagram for Cu–Co–Si alloy. The software calculates the equilibrium phase diagram based on the thermodynamic properties of the system [31]. The phase diagram of Cu–Co–Si ternary alloys at 450 °C and 1050 °C is calculated and shown in Fig. 1. Three alloys are designed and named as Cu–0.5Si, Cu–1.5Si and Cu–1Co–0.5Si in the following text. The nominal composition of the Cu–1Co–0.5Si alloy was designed to ensure that the Co and Si atoms can be completely dissolved into the Cu matrix at a solid solution temperature of 1050 °C, and the CoSi compound can be precipitated from the Cu matrix when aging at 450 °C. The Co-free alloys (Cu–0.5Si and Cu–1.5Si) were designed to investigate the influence of the Co addition on the microstructure and properties of Cu–Si alloys. The alloys were prepared by vacuum induction melting. Pure Cu (99.95%), Co (99.95%) and Si (99.99%) were used as starting materials. Table 1 shows the chemical compositions of the samples tested by inductively coupled plasma-atomic emission spectrometer. The as-cast ingots were subjected to solution treatment at 1050 °C for 8 h and subsequently quenched in water.

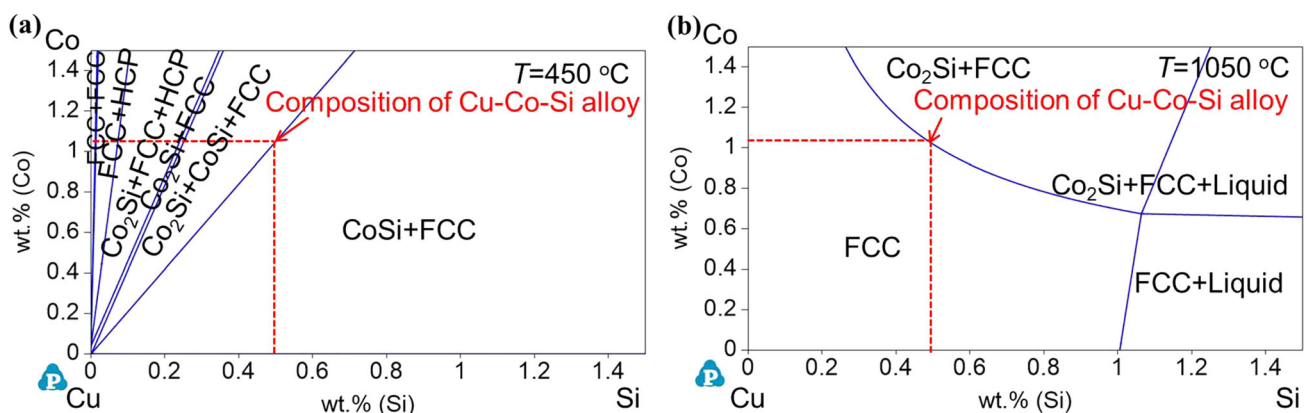


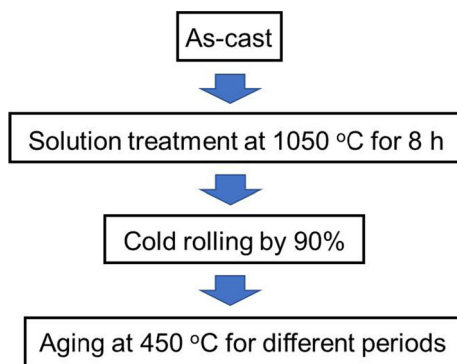
Figure 1 Phase diagram of Cu–Co–Si alloys with PANDAT softwareTM at **a** 450 °C; **b** 1050 °C.

Table 1 Experimental compositions of the designed alloys (wt.%)

Alloys	Co	Si	Cu
Cu-0.5Si	–	0.52	Bal.
Cu-1.5Si	–	1.51	Bal.
Cu-1Co-0.5Si	1.06	0.45	Bal.

Afterward, the specimens were cold rolled to a 90% reduction in thickness and then aged at 450 °C for different periods. The whole process flow was shown in Fig. 2.

Microhardness was measured by a HDX-1000 Vickers hardness tester under a load of 100 g and a loading time of 10 s. Each sample was measured five times to get an average value. Electrical resistance was measured utilizing a RTS-11 four-probe resistivity tester at 20 °C. Electrical resistance was calculated and transformed into electrical conductivity according to International Annealed Copper Standards (IACS). Phase identification was performed using X-ray diffraction (XRD) equipped with a Cu

**Figure 2** The schematic illustration of the thermomechanical treatment process.

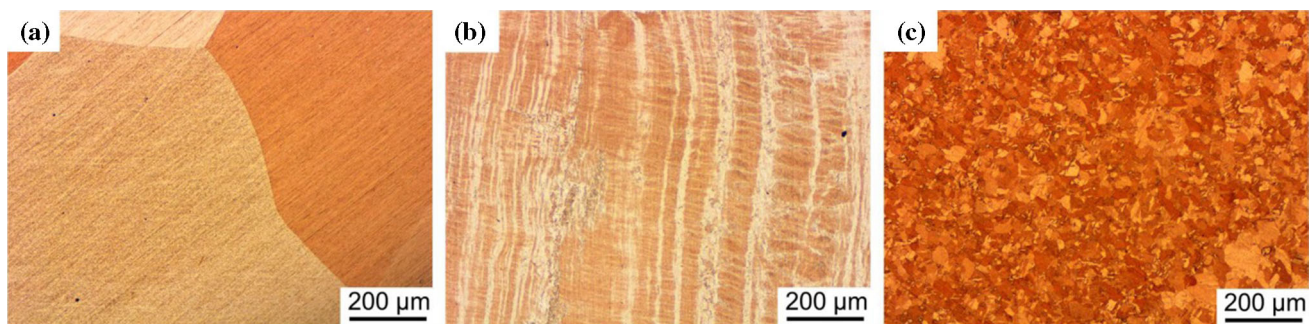
target operating at 40 kV at room temperature. The XRD sample for analyzing the phase structure of the precipitates was obtained by electrolytic corrosion of the Cu–Co–Si alloy [25]. The morphology of the precipitates was investigated by an optical microscope and a transmission electron microscope (TEM). The thin foils for TEM were prepared by Struers Tenpol-5 twin-jet unit electropolishing equipment using a solution of 25% HNO₃ + 75% CH₃OH with a voltage of 7 V at – 30 °C.

Results

Microstructure characterization

The optical microstructure of the Cu-0.5Si and Cu-1.5Si alloys is shown in Figs. 3 and 4. The microstructure of both solution-treated Cu-Si alloys is dominated by equiaxed crystals with clear grain boundaries and no second phase is found, which means that Si atoms are almost dissolved in the matrix to form a supersaturated solid solution. After rolling by 90%, the grains of the alloys are elongated along the rolling direction and the microstructure is highly oriented. The elongated grains are recrystallized into equiaxed grains during aging. The average sizes of the grains in the aged Cu-0.5Si and Cu-1.5Si alloys are 30 and 37 μm, respectively.

The optical microstructure of the Cu-1Co-0.5Si alloy is shown in Fig. 5. The metallographic structure of the solid solution and rolling state of the alloy is similar to the Cu-Si alloys, but no grain with clear grain boundary is seen in the Cu-1Co-0.5Si alloy after aging for 16 h, which means that no obvious recrystallization can be observed in the microstructure.

**Figure 3** The optical micrograph of the Cu-0.5Si alloy **a** solid solution treated at 1050 °C for 8 h; **b** rolled with a reduction of 90%; **c** aged at 450 °C for 16 h.

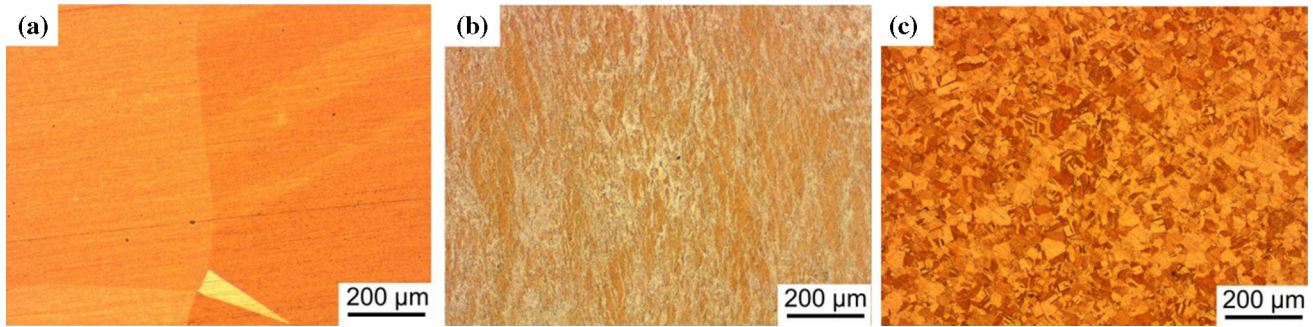


Figure 4 The optical micrograph of the Cu-1.5Si alloy **a** solid solution treated at 1050 °C for 8 h; **b** rolled with a reduction of 90%; **c** aged at 450 °C for 16 h.

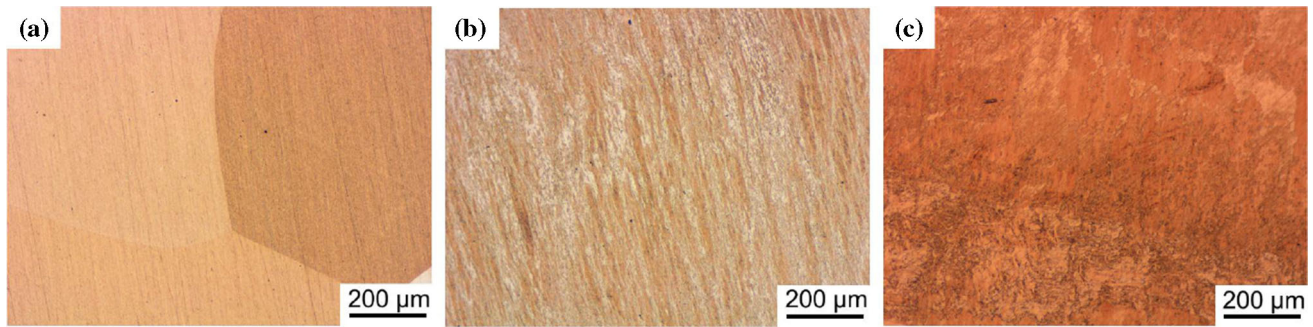


Figure 5 The optical micrograph of the Cu-1Co-0.5Si alloy **a** solid solution treated at 1050 °C for 8 h; **b** rolled with a reduction of 90%; **c** aged at 450 °C for 16 h.

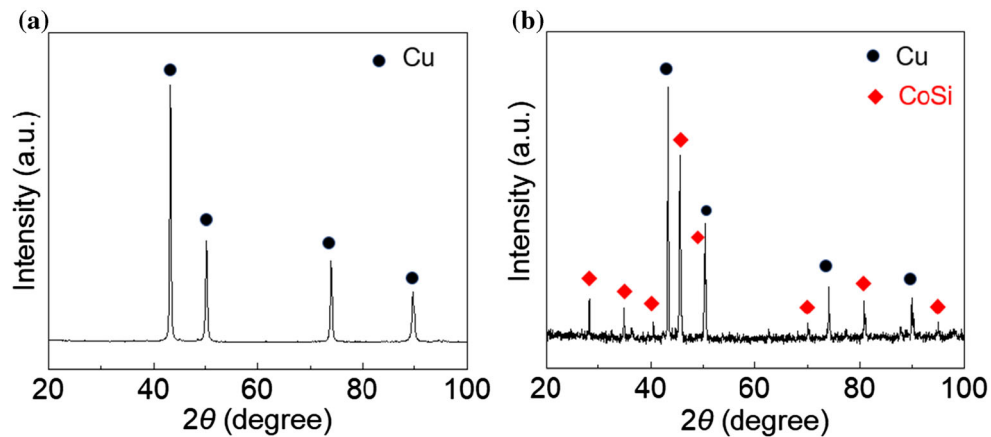


Figure 6 XRD patterns of **a** the aged Cu-1Co-0.5Si alloy and **b** the corroded Cu-1Co-0.5Si sample.

In order to identify the phase structure of the second phase, the XRD analysis of the aged Cu-Co-Si alloy was carried out. Figure 6a presents the XRD pattern of the aged Cu-1Co-0.5Si alloy. It can be seen that only the Cu diffraction peaks are detected due to the small volume fraction of the precipitates. Since the precipitates are not corroded by the hydrochloric acid and alcohol solution, they can be collected by corroding the Cu matrix and therefore the XRD signal

may be strong enough to determine the crystal structure [25]. Hence, the Cu-1Co-0.5Si alloy was corroded and the remained solid was analyzed by XRD. Figure 6b shows the corresponding XRD pattern of the aged Cu-1Co-0.5Si alloy after electrolytic corrosion. In addition to the Cu diffraction peaks, there are other diffraction peaks which agree well with the standard peaks of CoSi phase (ICSD No.50-

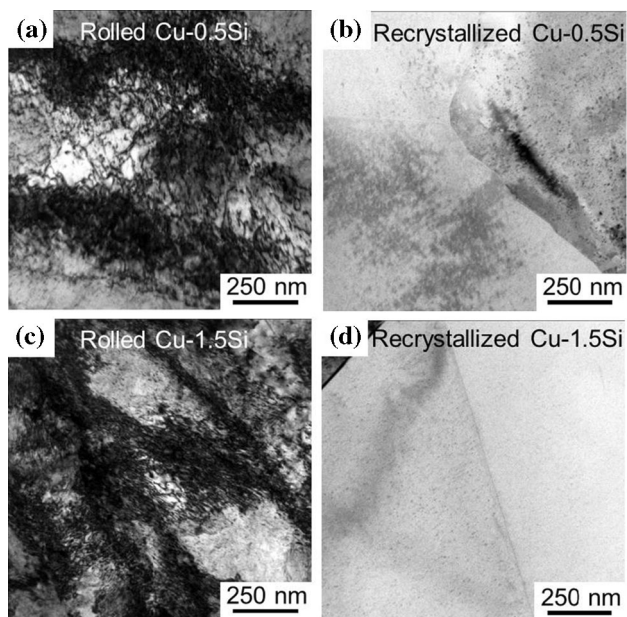


Figure 7 Bright-field TEM images of Cu-Si alloys **a** as-rolled Cu-0.5Si alloy; **b** aged Cu-0.5Si alloy at 450 °C for 16 h; **c** as-rolled Cu-1.5Si alloy; **d** aged Cu-1.5Si alloy at 450 °C for 16 h.

1337). Hence, the precipitate is clearly identified to be the CoSi phase.

Figure 7 shows the high density of dislocations in the rolled Cu-0.5Si and Cu-1.5Si alloys. However, the

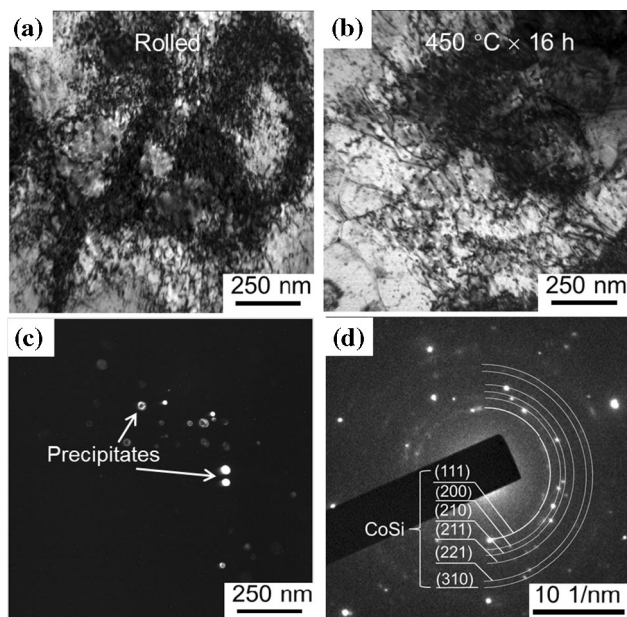


Figure 8 Bright-field TEM images of **a** rolled Cu-1Co-0.5Si alloy; **b** aged Cu-1Co-0.5Si alloy at 450 °C for 16 h; **c** dark-field TEM image of the aged Cu-1Co-0.5Si alloy at 450 °C for 16 h; **d** SADP of the nanoprecipitates in **c**.

strongly deformed microstructure is completely replaced by recrystallized grains after aging. Few dislocations and no second phase are observed in the recrystallized grains.

There is also a high density of dislocations in the rolled Cu-1Co-0.5Si (Fig. 8a). After aging at 450 °C for 16 h, the deformed microstructure is still held on (Fig. 8b). The dislocation density slightly decreases in the aged Cu-1Co-0.5Si compared to the cold-rolled microstructure (Fig. 8b). Plenty of nanoprecipitates are observed in the dark-field TEM image of the aged Cu-1Co-0.5Si (Fig. 8c). Figure 8d shows the selected area diffraction pattern (SADP) of the precipitates from the aged Cu-1Co-0.5Si alloy after electrolytic corrosion. Several diffraction rings and some dispersive strong spots are visible in the diffraction pattern. Those dispersive strong spots are from the remained Cu after electrolytic corrosion. The interplanar spacings corresponding to those diffraction rings are measured to be 0.25, 0.22, 0.21, 0.18, 0.15 and 0.14 nm, which agree with the spacings of (111), (200), (210), (211), (221) and (310) of CoSi phase, respectively. The diffraction pattern confirms the existence of Cu phase and CoSi phase, which is consistent with the XRD result.

In order to further analyze the crystal structure and composition of the nanoprecipitates, the CoSi phase was also characterized by TEM at a higher magnification. The structure and composition of a nanoprecipitate in the aged Cu-1Co-0.5Si are shown in Fig. 9. The length and width of the precipitate are 23 nm and 15 nm, respectively (Fig. 9a). The average diameter of the precipitates is 15.1 nm based on the measurement of more than 100 nanoprecipitates (Fig. 9b). The energy-dispersive spectrometer (EDS) results show that the precipitate is rich in Co and Si but poor of Cu. The atomic ratio of Co and Si is close to 1 (inset in Fig. 9g), which indicates that the precipitate should be CoSi compound. The EDS results also support the identification of CoSi precipitates by XRD and SADP tests in Figs. 6 and 8. There is only one set of diffraction spots in the corresponding fast Fourier transform (FFT) image of Fig. 9c, suggesting that the CoSi nanoprecipitate have the same orientation as the Cu matrix. Some misfit dislocations are located at the phase interface (Fig. 9f). Therefore, it can be deduced that the CoSi nanoprecipitate is semi-coherent with the Cu matrix.

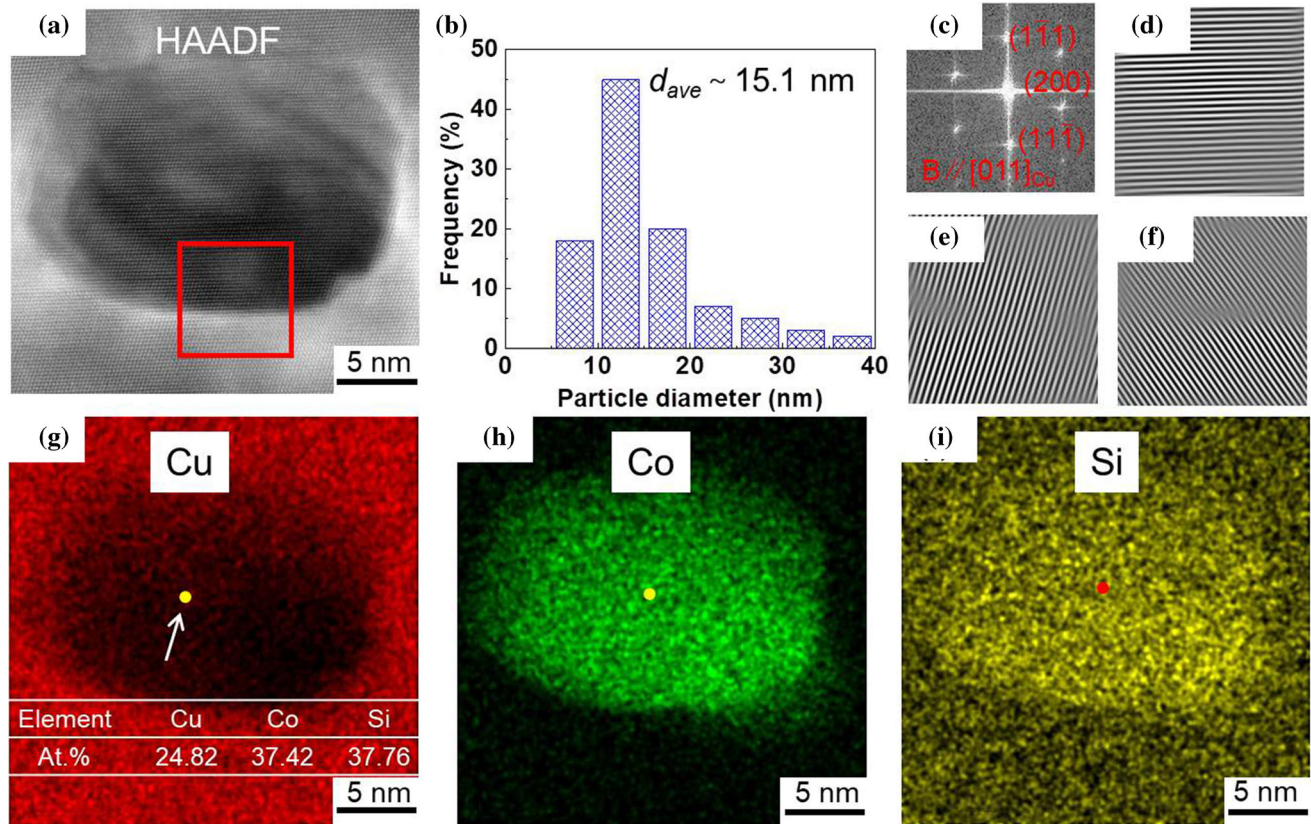
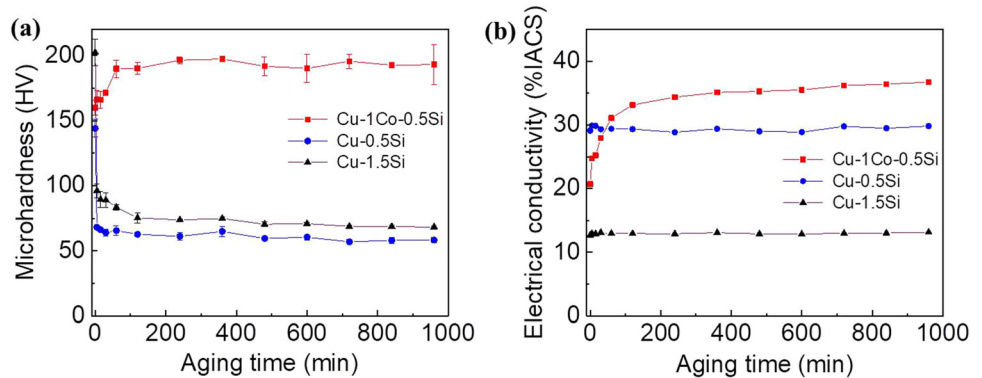


Figure 9 a High-angle annular dark-field (HAADF) image of a precipitate in the aged Cu-1Co-0.5Si alloy (taken from $\langle 011 \rangle_{Cu}$); b Diameter distribution of the precipitates; c FFT image of a; Inverse FFT patterns (d) using only $(1 \bar{1} 1)$, (e)

using only $(11\bar{1})$ and (f) using only (200) reflection; Elemental mappings of g Cu, h Co and i Si acquired from the area in a. The EDS result of the precipitate compositions is shown in the inset g.

Figure 10 a Hardness and b electrical conductivity of the designed alloys aged at 450 °C.



Hardness and electrical conductivity

The variation in hardness and conductivity of the tested alloys with aging time is shown in Fig. 10. The hardness of the rolled Cu-1Co-0.5Si alloy reaches a value of 160.07 HV, which is higher than the rolled Cu-0.5Si alloy but lower than the rolled Cu-1.5Si alloy. After aging treatment, the hardness of the

rolled Cu-Si alloys drops obviously in the first 5 min and then remains stable. The hardness of the aged Cu-1Co-0.5Si alloy increases with aging time and reaches a peak value of 190.04 HV at 2 h, which is more than twice times of the hardness of the Cu-0.5Si and Cu-1.5Si alloys.

The electrical conductivity of the rolled Cu-0.5Si, Cu-1.5Si and Cu-1Co-0.5Si alloys are 29.12%, 12.71%

and 20.70% IACS, respectively. The conductivity of the Cu-Si alloys remains almost unchanged during the aging process. In contrast, the electrical conductivity of the Cu-1Co-0.5Si alloy increases significantly within the first 2 h and then slowly. Compared with the rolled Cu-1Co-0.5Si alloy, the electrical conductivity of the alloy aged for 16 h is increased by 66.14%.

The results in Fig. 10 clearly exhibit that Co addition has a remarkably positive effect on the hardness and conductivity of the Cu-Si alloys. A good combination of hardness (190.04 HV) and electrical conductivity (34.39% IACS) can be obtained in the Cu-1Co-0.5Si alloy aged at 450 °C for 2 h.

Discussions

Thermodynamic analysis of compounds in the Cu-Co-Si alloy

In theory, the Co-Cu system with two similar fcc metals shows pronounced immiscibility in a solid phase, so that Cu and Co cannot form compounds [30]. But the Cu-Si and Co-Si can form intermetallic phases during the aging process [31, 32]. It has been reported that there are $\text{Cu}_{15}\text{Si}_4$, $\text{Cu}_{19}\text{Si}_6$, $\text{Cu}_{56}\text{Si}_{11}$, $\text{Cu}_{33}\text{Si}_7$ phases in the Cu-Si and Co_2Si , CoSi and CoSi_2 phases in the Co-Si [33]. When more than one phase may be precipitated in the alloy, the phase with the lower Gibbs energy (ΔG^θ) is more likely to precipitate during the aging process. The Gibbs energies of the seven phases are evaluated by the following equations [31, 32]:

$$\Delta G_{\text{Cu}_{33}\text{Si}_7}^\theta = -2660 - 5.59T \quad (1)$$

$$\Delta G_{\text{Cu}_{15}\text{Si}_4}^\theta = -5142 - 3.91T \quad (2)$$

$$\Delta G_{\text{Cu}_{19}\text{Si}_6}^\theta = -5065 - 4.51T \quad (3)$$

$$\Delta G_{\text{Cu}_{56}\text{Si}_{11}}^\theta = -4014 - 3.98T \quad (4)$$

$$\Delta G_{\text{CoSi}}^\theta = -48001 + 50.45T - 10.58T \ln T - 0.01T^2 - 389369.9T^{-1} \quad (5)$$

$$\Delta G_{\text{Co}_2\text{Si}}^\theta = -28546.8 - 24.99T - 0.79T \ln T - 0.015T^2 - 1419271.2T^{-1} \quad (6)$$

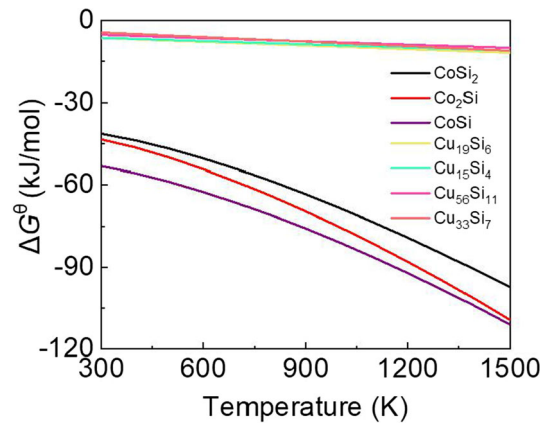


Figure 11 Gibbs free energy of the seven compounds in the Cu-Co-Si alloy as a function of temperature.

$$\Delta G_{\text{CoSi}_2}^\theta = -41239.2 + 116.62T - 20.18T \ln T - 0.0043T^2 - 63420.2T^{-1} \quad (7)$$

The ΔG^θ of the seven compounds in Cu-Co-Si alloy as a function of the temperature are shown in Fig. 11. The ΔG^θ of the four CuSi compounds are much higher than those of the three CoSi compounds. Among the three CoSi compounds, the CoSi intermetallic phase has the lowest Gibbs energy. Therefore, the CoSi intermetallic phase is thermodynamically stable and preferentially formed in the aged Cu-Co-Si alloy. This is consistent with the above experimental results.

The effect of CoSi precipitates on the properties

The hardness of the rolled Cu-1.5Si alloy is higher than that of the rolled Cu-0.5Si alloy due to the stronger solid solution strengthening effect produced by higher Si content [8]. Since the equilibrium solubility of Si in Cu matrix is 4.6 wt% at 450 °C [16], Si atoms should be dissolved in the Cu matrix, and no CuSi precipitate can be formed in the aged Cu-0.5Si and Cu-1.5Si alloys. The recrystallization during the aging consumes the high density of dislocations, resulting in the fast reduction in the hardness of both Cu-0.5Si and Cu-1.5Si. The consumption of dislocations leads to a slight recovery in the electrical conductivity since the resistance from dislocations is much weaker than that from dissolved atoms. When the recrystallization is completed, the hardness and electrical conductivity keep stable in the aged Cu-0.5Si and Cu-1.5Si. When adding Co into the Cu-Si

alloys, Co reacts with Si to form the CoSi nanoprecipitates in the aged Cu-1Co-0.5Si. The CoSi nanoprecipitates pin dislocation motion and prevent the recrystallization [34]. Therefore, a high density of dislocations are remained and plenty of nanoprecipitates are generated in the aged Cu-1Co-0.5Si. As a result, the hardness of the aged Cu-1Co-0.5Si increases and reaches a peak value of 190.04 HV at 2 h. At the same time, the precipitation of CoSi compound consumes the dissolved Si atoms in the Cu lattice, which significantly reduces the scattering level from dissolved solutes. So, the electrical conductivity of the aged Cu-1Co-0.5Si can be increased by 66.14% after aging for 16 h.

Conclusions

Cu-0.5Si, Cu-1.5Si and Cu-1Co-0.5Si alloys are designed and prepared to investigate the effect of Co addition on the microstructure and properties of Cu-Si alloys. The Cu-1Co-0.5Si alloy shows much higher hardness and better electrical conductivity than Cu-0.5Si and Cu-1.5Si. Co can react with the Si to form CoSi nanoprecipitates in the aged Cu-1Co-0.5Si. The presence of CoSi nanoprecipitates is sufficiently verified by the XRD, EDS and SADP results. The CoSi nanoprecipitates with an average diameter of 15.1 nm present a semi-coherent interface with the Cu matrix. The formation of CoSi nanoprecipitates pins dislocation motion prevents recrystallization and promotes precipitation of the dissolved Si. The benefits from Co alloying making both precipitate hardening and precipitation purifying result in the much excellent performance of the aged Cu-1Co-0.5Si than that of the Cu-0.5Si and Cu-1.5Si.

Acknowledgements

This work is financially supported by the National Natural Science Foundation of China (No. 11725210) and the Fundamental Research Funds for the Central Universities (2018XZZX001-05).

Author contributions

YF, JL and HW initiated the project. CL and XF prepared the Cu alloys and carried out the performance

tests. HY conducted the TEM characterization. FZ and LM conducted the alloy design and analysis. CL, JL and LM wrote the manuscript and all the authors contributed to the discussion and revision of the manuscript.

Data availability

The raw/processed data required to reproduce these findings cannot be shared at this time as the data also forms part of an ongoing study.

Declarations

Conflict of interest The author(s) declare that they have no competing interests.

References

- [1] Chalon J, Guerin JD, Dubar L, Dubois A, Puchi-Cabrera ES (2016) Characterization of the hot-working behavior of a Cu-Ni-Si alloy. *Mater Sci Eng A* 667:77–86. <https://doi.org/10.1016/j.msea.2016.04.061>
- [2] Semboshi S, Sato S, Iwase A, Takasugi T (2016) Discontinuous precipitates in age-hardening Cu-Ni-Si alloys. *Mater Charact* 115:39–45. <https://doi.org/10.1016/j.matchar.2016.03.017>
- [3] Choi JH (2012) Aging behavior and precipitate analysis of copper-rich Cu-Fe-Mn-P alloy. *Mater Sci Eng A* 550:183–190. <https://doi.org/10.1016/j.msea.2012.04.055>
- [4] Batra IS, Dey GK, Kulkarni UD, Banerjee S (2001) Microstructure and properties of a Cu-Cr-Zr alloy. *J Nucl Mater* 299(2):91–100. [https://doi.org/10.1016/s0022-3115\(01\)00691-2](https://doi.org/10.1016/s0022-3115(01)00691-2)
- [5] Zinkle SJ (2016) Applicability of copper alloys for DEMO high heat flux components. *Phys Scr*. <https://doi.org/10.1088/0031-8949/2015/t167/014004>
- [6] Guo X, Xiao Z, Qiu W, Li Z, Zhao Z, Wang X, Jiang Y (2019) Microstructure and properties of Cu-Cr-Nb alloy with high strength, high electrical conductivity and good softening resistance performance at elevated temperature. *Mater Sci Eng A* 749:281–290. <https://doi.org/10.1016/j.msea.2019.02.036>
- [7] Wang W, Kang H, Chen Z, Chen Z, Zou C, Li R, Yin G, Wang T (2016) Effects of Cr and Zr additions on microstructure and properties of Cu-Ni-Si alloys. *Mater Sci Eng A* 673:378–390. <https://doi.org/10.1016/j.msea.2016.07.021>

- [8] Li Y, Xiao Z, Li Z, Zhou Z, Yang Z, Lei Q (2017) Microstructure and properties of a novel Cu-Mg-Ca alloy with high strength and high electrical conductivity. *J Alloys Compd* 723:1162–1170. <https://doi.org/10.1016/j.jallcom.2017.06.155>
- [9] Lee E, Han S, Euh K, Lim S, Kim S (2011) Effect of Ti addition on tensile properties of Cu-Ni-Si alloys. *Met Mater Int* 17(4):569–576. <https://doi.org/10.1007/s12540-011-0807-7>
- [10] Jiang L, Fu H, Wang C, Li W, Xie J (2020) Enhanced mechanical and electrical properties of a Cu-Ni-Si alloy by thermo-mechanical processing. *Metall Mater Trans A* 51(1):331–341. <https://doi.org/10.1007/s11661-019-05507-3>
- [11] Hu T, Chen JH, Liu JZ, Liu ZR, Wu CL (2013) The crystallographic and morphological evolution of the strengthening precipitates in Cu-Ni-Si alloys. *Acta Mater* 61(4):1210–1219. <https://doi.org/10.1016/j.actamat.2012.10.031>
- [12] Zhang K, Yang J, Li J, Chen X, Zhou H, Liu P (2021) Effect of deformation and aging treatment on the microstructure and properties of Cu-0.45Cr-0.14Ti (wt.%) alloy. *J Alloys Compd*. <https://doi.org/10.1016/j.jallcom.2020.156776>
- [13] Krupinska B, Borek W, Krupinski M, Karkoszka T (2020) The influence of Ag on the microstructure and properties of Cu-Ni-Si alloys. *Materials*. <https://doi.org/10.3390/ma13153416>
- [14] Lei Q, Li Z, Dai C, Wang J, Chen X, Xie JM, Yang WW, Chen DL (2013) Effect of aluminum on microstructure and property of Cu-Ni-Si alloys. *Mater Sci Eng A* 572:65–74. <https://doi.org/10.1016/j.msea.2013.02.024>
- [15] Li Z, Xiao Z, Jiang Y, Lei Q, Xie J (2019) Composition design, phase transition and fabrication of copper alloys with high strength and electrical conductivity. *Chin J Nonferr Met* 29(9):2009–2049
- [16] Soldi L, Laplace A, Roskosz M, Gosse S (2019) Phase diagram and thermodynamic model for the Cu-Si and the Cu-Fe-Si systems. *J Alloys Compd* 803:61–70. <https://doi.org/10.1016/j.jallcom.2019.06.236>
- [17] Connetable D, Thomas O (2011) First-principles study of nickel-silicides ordered phases. *J Alloys Compd* 509(6):2639–2644. <https://doi.org/10.1016/j.jallcom.2010.10.118>
- [18] Cao Y, Han SZ, Choi E-A, Ahn JH, Mi X, Lee S, Shin H, Kim S, Lee J (2020) Effect of inclusion on strength and conductivity of Cu-Ni-Si alloys with discontinuous precipitation. *J Alloys Compd*. <https://doi.org/10.1016/j.jallcom.2020.156006>
- [19] Cheng JY, Tang BB, Yu FX, Shen B (2014) Evaluation of nanoscaled precipitates in a Cu-Ni-Si-Cr alloy during aging. *J Alloys Compd* 614:189–195. <https://doi.org/10.1016/j.jallcom.2014.06.089>
- [20] Lei Q, Li Z, Wang MP, Zhang L, Gong S, Xiao Z, Pan ZY (2011) Phase transformations behavior in a Cu-8.0Ni-1.8Si alloy. *J Alloys Compd* 509(8):3617–3622. <https://doi.org/10.1016/j.jallcom.2010.12.115>
- [21] Wu Y, Li Y, Lu J, Tan S, Jiang F, Sun J (2019) Effects of pre-deformation on precipitation behaviors and properties in Cu-Ni-Si-Cr alloy. *Mater Sci Eng A* 742:501–507. <https://doi.org/10.1016/j.msea.2018.11.045>
- [22] Wang C, Zhu J, Lu Y, Guo Y, Liu X (2014) Thermodynamic description of the Cu-Ni-Si system. *J Ph Equilibria Diffus* 35(1):93–104. <https://doi.org/10.1007/s11669-013-0277-3>
- [23] Li J, Huang G, Mi X, Peng L, Xie H, Kang Y (2019) Influence of the Ni/Co mass ratio on the microstructure and properties of quaternary Cu-Ni-Co-Si alloys. *Materials*. <https://doi.org/10.3390/ma12182855>
- [24] Geng Y, Li X, Zhou H, Zhang Y, Jia Y, Tian B, Liu Y, Volinsky AA, Zhang X, Song K, Wang G, Li L, Hou J (2020) Effect of Ti addition on microstructure evolution and precipitation in Cu-Co-Si alloy during hot deformation. *J Alloys Compd*. <https://doi.org/10.1016/j.jallcom.2019.153518>
- [25] Sun X, Jie J, Wang P, Qin B, Ma X, Wang T, Li T (2019) Effects of Co and Si additions and cryogenic rolling on structure and properties of Cu-Cr alloys. *Mater Sci Eng A* 740:165–173. <https://doi.org/10.1016/j.msea.2018.10.093>
- [26] Zhao Z, Zhang Y, Tian B, Jia Y, Liu Y, Song K, Volinsky AA (2019) Co effects on Cu-Ni-Si alloys microstructure and physical properties. *J Alloys Compd* 797:1327–1337. <https://doi.org/10.1016/j.jallcom.2019.05.135>
- [27] Chen Y, Dai A, Zhu Z (2016) Solution and aging treatment of Cu-Co-Si-Zr alloy. *Spec Cast Nonferr Alloys* 36(7):781–784
- [28] Toda T (1970) Critical cooling rates determined by Jominy tests in age-hardening Cu-Cr, Cu-Be and Cu-Co₂Si alloys. *Trans Jpn Inst Met* 11(1):24–29. <https://doi.org/10.2320/matertrans1960.11.24>
- [29] Lendvai J, Ungar T, Kovacs I, Albert B (1988) Precipitation processes in Cu-Co-Si alloys. *J Mater Sci* 23(11):4059–4065. <https://doi.org/10.1007/bf01106835>
- [30] Kubista J, Vrest'al J (2000) Thermodynamics of the liquid Co-Cu system and calculation of phase diagram. *J Ph Equilib* 21(2):125–129. <https://doi.org/10.1361/105497100770340165>
- [31] Zhang L, Du Y, Xu H, Pan Z (2006) Experimental investigation and thermodynamic description of the Co-Si system. *Calphad* 30(4):470–481. <https://doi.org/10.1016/j.calphad.2006.06.001>

- [32] Shin D, Saal JE, Liu Z-K (2008) Thermodynamic modeling of the Cu-Si system. *Calphad* 32(3):520–526. <https://doi.org/10.1016/j.calphad.2008.05.003>
- [33] Yan XY, Chang YA (2000) A thermodynamic analysis of the Cu-Si system. *J Alloys Compd* 308:221–229. [https://doi.org/10.1016/s0925-8388\(00\)00983-x](https://doi.org/10.1016/s0925-8388(00)00983-x)
- [34] Li M, Wang H, Guo Y, Wang H, Zheng D, Shan J, Chang Y (2020) Microstructures and mechanical properties of the novel Cu-Cr-Zr-Fe-Ti-Y alloy for fusion reactor. *J Nucl Mater.* <https://doi.org/10.1016/j.jnucmat.2020.152063>

Publisher's Note Springer Nature remains neutral with regard to jurisdictional claims in published maps and institutional affiliations.